A Multi-Sensor Fusion Self-Localization System of a Miniature Underwater Robot in Structured and GPS-Denied Environments

Huiming Xing, *Member, IEEE*, Yu Liu, Shuxiang Guo, *Fellow, IEEE*, Liwei Shi, *Member, IEEE*, Xihuan Hou, Wenzhi Liu, and Yan Zhao, *Member, IEEE*

***Abstract*—Aiming to deal with underwater localization for small-size robots in GPS-denied and structured environment, this paper proposed a novel multi-sensor fusion-based self-localization system using low-cost sensors. Based on multi-sensor information fusion, an Extended Kalman Filter (EKF) is utilized to synthesize the multi-source information from an Inertial Measurement Unit (IMU), optical flow, pressure sensor and ArUco markers, which enables the robot obtain a highly precise positioning. This method also can reduce the location drift over time owing to the loss of markers in pure markers-based localization. Specially, a velocity correction model is proposed using the angle information obtained by IMU, which can compensate optical flow-based velocity estimation errors caused by robot posture changes. Finally, to validate the performance of the proposed self-localization system, simulations are conducted using Gazebo simulator on the robot operating system (ROS). Moreover, a series of experiments in an indoor swimming pool are presented. Results of the proposed method and dead reckoning are compared in simulation and experiment to demonstrate the robustness and feasibility of the proposed localization system.**

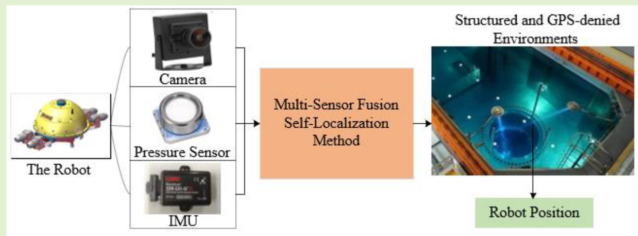

Schematic diagram of multi-sensor fusion self-localization system

***Index Terms*—Bio-inspired robot, multi-sensor fusion, marker- assisted localization, underwater self-localization system.**

I. Introduction

IN RECENT decades, underwater detection and localization using underwater sensor networks [1], [2] have a great development. But these methods are the most important technologies to guide the robot to implement autonomous operation tasks [3], [4] in open and wide oceans. In narrow and structured spaces, such as nuclear reactor pool, underwater self-localization methods [5], [6] are necessary for the autonomous underwater vehicles and underwater robots. In Fig.1, the robot is operating in the nuclear reactor pool.

Now most underwater self-localization researchers are focused on the deep-seas environment for large AUVs. As shown in TABLE I, these researches are mainly divided into three categories: Inertial Navigation System (INS), Acoustic Beacon-based System (ABS), GPS-based system and Simultaneous Localization and Mapping (SLAM). INS method is also called dead-reckoning [7], [8], which is calculate the vehicles moving distance using the direction and velocity obtained by Inertial Measurement Unit (IMU) and Doppler Velocity Log (DVL), respectively. The acoustic localization system [9] acquires the location by measuring the time of flight of signals from acoustic beacons or modems to perform navigation. The two methods all need equipment with large size and high power, which is not suitable for the miniature underwater robot. GPS-based positioning method [10], [11] is not used in underwater environments. SLAM-based localization method [12], [13] is realized with surrounding environment features detection in visual measurement or imaging sonar. But in the nuclear reactor pool, the bottom and wall of pool are smooth monochromatic planes, and it is difficult

Manuscript received September 8, 2021; revised October 10, 2021; accepted October 13, 2021. Date of publication October 15, 2021; date of current version November 30, 2021. This work was supported in part by the Fundamental Research Funds for the Central Universities of Ministry of Education of China under Grant XK2040021004004 and Grant XK2040021004014, in part by the Graduate Technological Innovation Project of Beijing Institute of Technology under Grant 2018CX10022, in part by the National High Technology Research and Development Program of China under Grant 2015AA043202, in part by the National Natural Science Foundation of China under Grant 61773064 and Grant 61503028, and in part by the preferential funding for Post-doctoral Research Projects of Hebei Province of China under Grant B2020003020. The associate editor coordinating the review of this article and approving it for publication was Prof. Danilo Demarchi. *(Corresponding authors: Shuxiang Guo; Liwei Shi.)*

Huiming Xing and Wenzhi Liu are with the College of Intelligent Systems Science and Engineering, Harbin Engineering University, Harbin, Heilongjiang 150001, China.

Yu Liu, Liwei Shi, and Xihuan Hou are with the Key Laboratory of Convergence Medical Engineering System and Healthcare Technology, Ministry of Industry and Information Technology, Beijing Institute of Technology, Beijing 100081, China (e-mail: shiliwei@bit.edu.cn).

Shuxiang Guo is with the Key Laboratory of Convergence Medical Engineering System and Healthcare Technology, Ministry of Industry and Information Technology, Beijing Institute of Technology, Beijing 100081, China, and also with the Faculty of Engineering, Kagawa University, Takamatsu 761-0396, Japan (e-mail: guo.shuxiang@eng.kagawa-u.ac.jp).

Yan Zhao is with the School of Mechanical Engineering, Hebei University of Technology, Tianjin 300401, China.

Digital Object Identifier 10.1109/JSEN.2021.3120663

1558-1748 © 2021 IEEE. Personal use is permitted, but republication/redistribution requires IEEE permission.
See https://www.ieee.org/publications/rights/index.html for more information.

Authorized licensed use limited to: Harbin Engineering Univ Library. Downloaded on December 01,2021 at 02:26:24 UTC from IEEE Xplore. Restrictions apply.

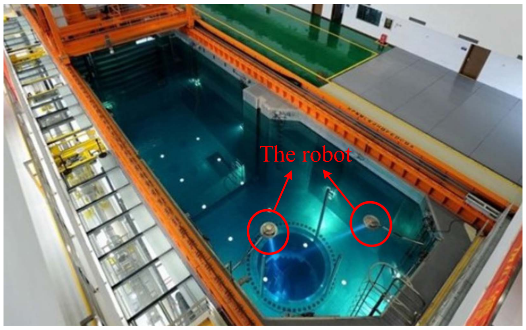

Fig. 1. Overview of the robot operation in the nuclear reactor pool.

to detect features. Therefore, autonomous underwater self-localization method in structured and GPS-denied environments are more challenging and difficult than in the widely deep sea.

Unlike the field environment, such as the sea and the river, the water in structured environments (the nuclear reactor pool etc.) are much clearer, which make vision-based approach [14]–[16] become feasible. As shown in TABLE I, except the advantage of low-cost sensors and low power consumption, vision-based localization is a feasible method for the miniature underwater robot [17], [18] with limited computational capacities and energy. A planar marker-based localization system [19] has been built in the robotic fish with the cheap webcam and the ARM processor. And the accurate absolute position information can be obtained by the 30 markers in the bottom of the aquarium. Another research [20] also used a coded map covered on the bottom in a water tank to estimate position of the robot. More importantly, in order to improve the stability and accuracy of vision-based localization, many researches combine vision-based method with inertial navigation. Karras *et al*. proposed the state estimation module [21] using IMU, pressure sensor and a down-looking camera. The pose, velocity and acceleration were fused by complementary filter. Meanwhile, ArUco markers were used to correct the accumulated error, but the velocity correction is not presented. Jongdae *et al*. proposed a AUVs self-localization method [22] using visual measurements of underwater structures and artificial landmarks. The particle filter was exploited to fuse data from IMU, DVL, markers and attitude and heading reference system (AHRS). This method needs to extracted geometry information of the target structure to compare with pre-generated synthetic observations, which greatly increased the complexity of the system and reduced the robustness of the system. Besides, compared with a down-looking camera, the FOV (field of vision) limitation of a forward-looking camera in this method reduced the probability that the robot cannot capture the markers, but it led to the localization drift easily.

In this paper, a multi-sensor fusion-based self-localization system of a miniature underwater robot is proposed to generate high-precision position online using low-cost and small-size sensors in structured and GPS-denied environment. Considering the efficiency and accuracy of Extend Kalman Filter (EKF), Unscented Kalman Filter (UKF) and Particle Filter (PF), EKF is used to fuse the multi-source information, including the pose and position from ArUco markers, heading angle from IMU, corrected velocity from optical flow and depth from pressure sensor, to reduce the location drift over time owing to the loss of markers in pure markers-based localization. To help the reader to understand this method, a detailed notations introduce is given in TABLE II.

TABLE I
DISTINCTIVE CHARACTERISTICS OF EXISTING LOCALIZATION METHODS

Methods	Main distinctive characteristics
INS+DVL	long time self-localization in water, position error accumulation, sensors with large size and high power
ABS	positioning using multiple acoustic beacons, limited application, sensors with large size and high power
GPS	wide application without underwater
SLAM	Suitable for scenarios with obvious features, heavy computation
Vision-based localization	low-cost and low power consumption, widely used in many scenarios by fusion with other sensors

TABLE II
NOTATIONS IN PROPOSED APPROACH

Notations	Descriptions
$P_m^a=(x_m^a,y_m^a,z_m^a)$	marker center position in coordinate *m*
$O_m^a=(\theta_m^a,\varphi_m^a,\psi_m^a)$	marker orientation in coordinate *m*
$P_m^c=(x_m^c,y_m^c,z_m^c)$	camera position in coordinate *m*
$O_m^c=(\theta_m^c,\varphi_m^c,\psi_m^c)$	camera orientation in coordinate *m*
$R(O_m^a)$	rotation matrix from coordinate a to m
f	the focal length of the camera
h	the distance from camera from the pool bottom
FOV	the field of view
AB_x, AB_y	distances of AB in x and y of image plane
$A'B'_x$, $A'B'_y$	the distances in object plane
φ , θ, ψ ,	roll, yaw and pitch of the robot
$s(k)$	the states vector
$f(s(k),k)$	the nonlinear system function
$\theta(k)$, $v(k)$	yaw angle and velocity of robot
$\sigma(k)\sim N(0,Q(k))$	the process noise
$m(k)$	the measurement vector
$h(s(k))$	measurement function
$\upsilon(k)\sim N(0,R(k))$	the measurement noise
$Q(k)$	the process noise covariance matrix
$R(k)$	the measurement noise covariance matrix
P_k	the state covariance matrix
K_k	the Kalman gain matrix
F_k	Jacobi matrices of the nonlinear system function
H_k	Jacobi matrices of the measurement function

Authorized licensed use limited to: Harbin Engineering Univ Library. Downloaded on December 01,2021 at 02:26:24 UTC from IEEE Xplore. Restrictions apply.

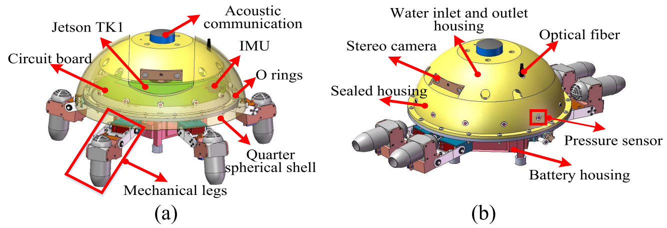

Fig. 2. Overview of the miniature underwater robot. (a) Crawling mode; (b) swimming mode.

Fig. 3. Main components of the proposed robot.

The rest of this paper is organized as follows. Section II gives robot platform. Section III presents EKF-based multi-sensor fusion-based self-localization system, including ArUco marker-based mapping and localization, velocity measurement and correction, EKF-based multi-source information fusion. Section IV and Section V conducted Simulations and experiments, respectively. Section VI concludes this paper.

II. Robot System Description

A. Overview of the Underwater Robot

Aiming at performing tasks in structured environments, a turtle-inspired spherical underwater robot [23]–[27] is developed. As shown in Fig. 2 (a), the robot is shaped like a sphere and the well-symmetry benefits underwater modeling and resistance to water turbulent. An intermediate plate divides it into two parts. The upper spherical part is composed of a sealed housing and an inlet and outlet housing that is used to regulate zero-buoyancy in water. The sealed housing consists a circuit system, processers, IMU, and pressure sensors. The acoustic communication and binocular camera are mounted on the upper part. The lower part consists of a detachable battery housing and a multi-vector water-jet propulsion system which is composed of four mechanical legs. Each leg has three joints actuated by servomotors. A downward-looking camera is equipped on the intermediate plate. Two servomotors are also installed on the plate to drive the opening and closing of two quarter-spherical hulls. As shown in Fig.2 (a), the robot can crawl on the pool floor in structured environment, such as a nuclear reactor pool. Also, the robot can swim between task waypoints as shown in Fig. 2(b).

B. Main Components of the Robot

According to application requirements, main components of the robot is shown in Fig. 3. It is divided into five components, including information processing, sensor, driving, communication and energy supply system.

The information processing system mainly performs tasks, such as sensor data collection and processing, robot position and pose control. Due to the limited power consumption and narrow space of the miniature underwater robot, NIVIDA Jetson TK1 is selected as the core processor and it is assisted by STM32F407VET6 microcontrollers to consider the efficiency of data processing. The robot is automatically operating on a Linux system, which communicates with the remote computer via an optical fiber cable. The sensing system completes tasks, such as sensing its own state and perceiving the surrounding environment. A low-cost down-looking camera fixed in a 3D-printed waterproof housing, is mounted to the left side of the robot, and used to acquire images in the bottom of tank. IMU is arranged in the sealed housing, and acquire the pose of the robot. Furthermore, a binocular camera is used to perceive obstacles ahead and a pressure sensor is utilized to calculate the distance between the robot and the water surface.

The multi-vector water-jet driving system is the basis of the robot movement in water. It is composed of four mechanical legs actuated by servo motors and water-jet thrusters. Each leg with three joints has three Degrees of Freedom (DoF) and the thruster is fixed on the leg. Four legs are radially free distributed around the robot with high symmetry, which composed the multi-vector water-jet propulsion system. Energy supply system provides the power for the whole robot system. The system has three 7.4V Li batteries with a total capacity of 13200mAh, which are processed by circuit modules to meet the different voltage requirements of different subsystems. The communication system includes acoustic communication and optical fiber communication. According to the needs of robot image transmission and multi-source data transmission, optical fiber is used to communicate with the remote computer.

III. EKF-Based Multi-Sensor Fusion Self-Localization System

This section presents EKF-based multi-source information fusion self-localization system. The acquisition and processing of pose information and velocity from ArUco markers and optical flow are introduced in detail. Then, multi-source information from IMU, optical flow, ArUco markers and pressure sensor is used to estimate the robot state using EKF. The schematic diagram of the proposed localization system is shown in Fig. 4.

A. ArUco Marker-Based Mapping and Localization

According to the discussion above, the position information obtained by ArUco makers [28] has high accuracy, which leads its higher credibility and priority in the localization system. Fig. 5(a) shows the successful detection of ArUco markers. But this method is easily affected by the light intensity. The low light intensity makes the environment dark, so the image is unclear and the visual features is not obvious. It is hard

Authorized licensed use limited to: Harbin Engineering Univ Library. Downloaded on December 01,2021 at 02:26:24 UTC from IEEE Xplore. Restrictions apply.

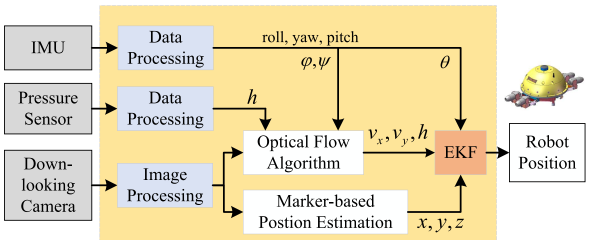

Fig. 4. Schematic diagram of self-localization system.

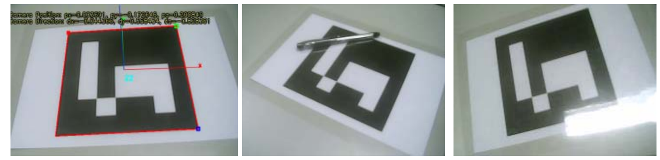

(a) (b) (c)

Fig. 5. Detection of ArUco markers. (a) Normal detection, (b) abnormal detection with shelter, (c) abnormal detection caused by reflection.

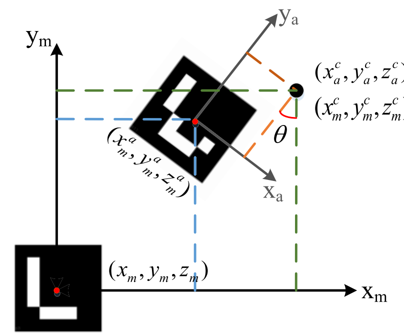

Fig. 6. The schematic diagram of coordinate transformation.

to detect the corners in optical flow method and recognize ArUco Markers. However, most of the nuclear pool have a good light intensity, and the clear water leads the markers identification easily. Therefore, the marker arrays are widely employed in featureless indoor environments such as a shallow test tank [29], such as the nuclear reactor pool. It is also suitable to correct the drift of the inertial navigation system.

ArUco library contains 1024 images that modified by different internal binary codes and assigned different numbers. And the marker can be uniquely identified by its code, which enables it to have the ability to provide detection, recognition and six DOF pose information of camera. Since the robot is not positioned at a fixed point, but over a large range, a series of ArUco markers which are arranged irregularly at the bottom of the pool are utilized in the proposed localization system. Therefore, the relative position of these markers is required. In other words, the map containing the location information of these markers needs to be determined in advance. Building a precise ArUco map is a vital component in the algorithm. One of the most intuitive methods is to apply visual information to complete the automatic mapping process. To be specific, if one marker is utilized as a reference frame, each frame captured by the camera should ensure that at least two markers exist at the same time, and at least one of them also exists in the previous frame, and so on, the relative position between each marker is obtained [30]. Then, the pose of camera can be calculated when any marker presents in the field of view.

The ArUco marker coordinate system is defined as a, and map coordinate system is defined as m, which is coincided with the coordinate of the first detected marker. Thus, the center position and orientation of the marker in coordinate m are $P_m^a = (x_m^a, y_m^a, z_m^a)$ and $O_m^a = (\theta_m^a, \varphi_m^a, \psi_m^a)$, respectively. And the position and orientation of the camera in coordinate m are $P_m^c = (x_m^c, y_m^c, z_m^c)$ and $O_m^c = (\theta_m^c, \varphi_m^c, \psi_m^c)$, respectively. The position and orientation of camera that calculated by markers in coordinate a are $P_a^c = (x_a^c, y_a^c, z_a^c)$ and $O_a^c = (\theta_a^c, \varphi_a^c, \psi_a^c)$. The plane schematic diagram of coordinate transformation is shown in Fig. 6. And the relationship of them is described as follows.

$$O_m^c = O_m^a + O_a^c \tag{1}$$

$$P_m^c = P_m^a + R(O_m^a)P_a^c \tag{2}$$

Since these irregular ArUco markers are all fixed on the flat ground, their height roll and pitch value equal to zero, that means, $z_m^a = 0$, $\varphi_m^a = 0$, $\psi_m^a = 0$. So, the $R(O_m^a)$ is obtained.

$$R(O_m^a) = \begin{bmatrix} \cos(\theta) & \sin(\theta) & 0 \\ -\sin(\theta) & \cos(\theta) & 0 \\ 0 & 0 & 1 \end{bmatrix} \tag{3}$$

Finally, O_m^c and P_m^c, also the pose of camera can be obtained from the above analysis. Considering that there may be more markers in a frame at the same time, the camera position calculated by each marker should be identical in a perfectly ideal situation. However, the error often exists. In this case, the pose information calculated by different markers is averaged to be the final and accurate value. The position of robot can also be derived from this information.

ArUco marker occupies little computational resources and provides the pose information of the camera with high precision, markers will not appear in the field of view all the time. Sometimes, when it appears in the field of view, it is challenge to recognize the markers because of the shelter or reflection, as shown in Fig. 5(b) and Fig. 5(c). Therefore, it is straightforward to consider obtaining stable positioning result with additional sensors, and ArUco marker-based localization is used to correct errors when they occur in the field of view and can be identified. So, the data processing from other sensors is introduced in the rest of this section.

B. Velocity Measurement and Correction

Optical flow is used to find the corresponding relationship between the previous frame and the current frame using the change of pixels in the time domain, then calculate the motion information of the robot between adjacent frames. In this paper, a down-looking camera is mounted on the robot to estimate the moving information of the robot.

A traditional Pyramid Lucas-Kanade optical flow method [31] is applied to proposed localization method.

Authorized licensed use limited to: Harbin Engineering Univ Library. Downloaded on December 01,2021 at 02:26:24 UTC from IEEE Xplore. Restrictions apply.

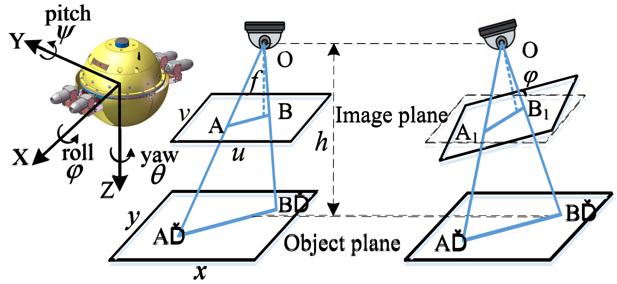

Fig. 7. Schematic diagram of velocity measurement by optical flow.

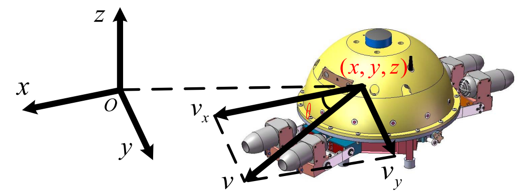

Fig. 8. State model of system.

The schematic diagram of calculating velocity by optical flow is shown in Fig. 7. Point O is the optic center of the camera, A is a feature point in the image, and B is the same feature point in another frame. The motion velocity of camera can be obtained from the distance of the same feature point in the different frame. In addition, f is the focal length of the camera, and h is the distance of the camera from bottom of the pool. Set FOV as the field of view, the velocity of camera can be calculated as below.

$$\frac{AB_x}{A'B'_x} = \frac{f}{h} = \frac{AB_y}{A'B'_y} \tag{4}$$

$$velocity_x = \frac{A'B'_y}{\Delta t} = \frac{|u_B - u_A| \cdot h}{f \cdot \Delta t} \tag{5}$$

$$velocity_y = \frac{A'B'_y}{\Delta t} = \frac{|v_B - v_A| \cdot h}{f \cdot \Delta t} \tag{6}$$

where AB_x, AB_y are the distances of AB in the x and y directions in image plane, respectively, and $A'B'_x, A'B'_y$ are the distances in object plane.

During the robot movement in water, the uneven distribution and water flow may cause the roll and pitch of the robot. As shown as in Fig. 7, the image plane of down-looking camera is not parallel to the object plane. Then, the estimated velocity of the robot is inaccurate. Therefore, an IMU-based corrected velocity estimated method is proposed by Equations (7)-(10).

$$AB_x = A_1B_{1x} - \varphi \cdot \frac{row}{FOV} \tag{7}$$

$$AB_y = A_1B_{1y} - \psi \cdot \frac{col}{FOV} \tag{8}$$

$$velocity_x = \frac{\left(\left|u_{B_1} - u_{A_1}\right| - \varphi \cdot \frac{row}{FOV}\right) \cdot h}{f \cdot \Delta t} \tag{9}$$

$$velocity_y = \frac{\left(\left|v_{B_1} - v_{A_1}\right| - \psi \cdot \frac{col}{FOV}\right) \cdot h}{f \cdot \Delta t} \tag{10}$$

where row, col are number of image rows and columns, respectively. And φ, ψ can be measured by IMU. Thus, the velocity of the robot is calculated.

C. EKF-Based Multi-Source Information Fusion

According to the previous discussion, when marker is not detected, inertial navigation is adopted to realize real-time self-localization. Therefore, optical flow technology and IMU are exploited for pose and position estimation. EKF is suitable for nonlinear system, and has a good real-time performance which is used to improve the proposed localization accuracy. The optimal estimated value of current state is obtained by the previous state estimation and the current state observation. In this process, the state model and observation model are essential to be established firstly.

1) State Model: considering to obtain the localization information of the robot, $s(k) = [x(k), y(k), z(k), \theta(k), v(k)]^T$ is set as the state vector of the system. As shown in Fig. 8, It consists of position in the world coordinate system, yaw angle and velocity of the robot. The system equation is given in the following form:

$$\begin{aligned} s(k) &= f(s(k-1), k-1) \\ &= \begin{bmatrix} x(k-1) + v(k-1) \cdot \Delta t \cdot \cos\theta \\ y(k-1) + v(k-1) \cdot \Delta t \cdot \sin\theta \\ z(k-1) \\ \theta(k-1) \\ v(k-1) \end{bmatrix} + \sigma(k-1) \end{aligned} \tag{11}$$

where $f(s(k), k)$ is the nonlinear system function, $\theta(k)$ and $v(k)$ are yaw angle and velocity of robot at time k, respectively. $\sigma(k)$ is the process noise which is assumed as Gaussian white noise and $\sigma(k) \sim N(0, Q(k))$, Δt is system sampling interval.

2) Measurement Model: In robot localization system, sensors are employed to refine the predicted position, including camera, pressure sensor and onboard IMU. Here are two situations: (1) the ArUco marker is captured and recognized; (2) ArUco maker is not recognized. Without ArUco marker-assisted localization, depth data from pressure sensor, yaw angle from IMU and velocity from optical flow can be used and the measurement vector is $m(k) = [z(k), \theta(k), v(k)]^T$. If the robot captured and recognized ArUco maker, the measurement vector is $m(k) = [x(k), y(k), z(k), \theta(k), v(k)]^T$. And the measurement equation is given as follows:

$$m(k) = h(s(k), k) + v(k) \tag{12}$$

where $h(s(k))$ is measurement function, $v(k)$ is assumed to Gaussian white noise in measurement and $v(k) \sim N(0, R(k))$.

With the system model described above, the depth, yaw angle and velocity are fused together to achieve localization. Although data acquisition from sensors is normally at a high frequency, the continuous localization trajectory does not exist in practical navigation applications. Therefore, EKF uses the current estimated state at each time step k as a linearization

Authorized licensed use limited to: Harbin Engineering Univ Library. Downloaded on December 01,2021 at 02:26:24 UTC from IEEE Xplore. Restrictions apply.

point [32]. And EKF algorithm is described as follows:

$$\hat{s}_{k|k-1} = F_k \hat{s}_{k-1} \tag{13}$$

$$P_{k|k-1} = F_{k-1} P_{k-1} F_{k-1}^T + Q(k) \tag{14}$$

$$K_k = P_{k|k-1} H_k^T (H_k P_{k|k-1} H_k^T + R(k))^{-1} \tag{15}$$

$$\hat{s}_k = \hat{s}_{k|k-1} + K_k (m_k - h(\hat{s}_{k|k-1})) \tag{16}$$

$$P_k = (I - K_k H_k) P_{k|k-1} \tag{17}$$

where, F_k and H_k are Jacobi matrices of the non-linear system function $f(s(k), k)$ and measurement function $h(s(k), k)$. $Q(k)$ is the process noise covariance matrix and $R(k)$ is the measurement noise covariance matrix. P_k is the state covariance matrix and K_k is the Kalman gain matrix. Besides, $\hat{}$ stands for estimate value. $Q(k)$ and $R(k)$ are the values reflecting process noise and measurement noise, respectively, and they are unable to be calculated by theoretical derivation and are often tuned experimentally by a trial-and-error method. The Jacobi matrices F_k and H_k are calculated as follows:

$$F_k = \nabla f(s(k), k) = \frac{\partial f(s(k), k)}{s(k)} = \begin{bmatrix} 1 & 0 & 0 & v \cdot \Delta t \cdot \cos\theta & \Delta t \cdot \sin\theta \\ 0 & 1 & 0 & -v \cdot \Delta t \cdot \sin\theta & \Delta t \cdot \cos\theta \\ 0 & 0 & 1 & 0 & 0 \\ 0 & 0 & 0 & 1 & 0 \\ 0 & 0 & 0 & 0 & 1 \end{bmatrix} \tag{18}$$

$$H_k = \nabla h(\mathbf{x}(k), k) = \frac{\partial h(\mathbf{x}(k), k)}{\partial \mathbf{x}(k)} = \begin{cases} \begin{bmatrix} 1&0&0&0&0 \\ 0&1&0&0&0 \\ 0&0&1&0&0 \\ 0&0&0&1&0 \\ 0&0&0&0&1 \end{bmatrix}, & \text{if ArUco is recognized} \\ \begin{bmatrix} 0&0&1&0&0 \\ 0&0&0&1&0 \\ 0&0&0&0&1 \end{bmatrix}, & \text{if ArUco is not recognized} \end{cases} \tag{19}$$

where, H_k is determined by whether the ArUco marker is recognized. The partial derivative of these Jacobi matrices is relatively easy to be calculated and it is not necessary to use UKF or PF. Therefore, the computational complexity of EKF is easier than UKF and PF.

D. Online Self-Localization Strategy

Generally, with key information extracted from sensors, the proposed EKF-based self-localization approach synthesizes the multi-source information to realize the online self-localization system with low-cost sensors and low power consumption hardware platform. In addition, other sensors can be easily extended to this system to further improve accuracy and redundancy. As illustrated in Fig. 9, initially the robot does not obtain its own position, and maybe none of marker exists in the field of view. Thus, the origin of the world coordinate system is defined as the projection point of the robot initial center position on the two-dimensional ground, and the vertical ground upward is the positive direction of the Z-axis.

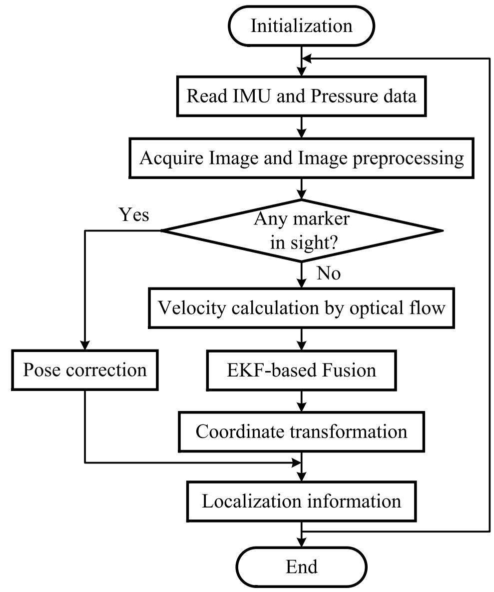

Fig. 9. Flowchart of the online self-localization system.

The direction in which the yaw angle equals to zero is the positive direction of the X-axis, and the definition of Y-axis satisfies the right-hand rule. When the marker does not appear, only the yaw angle provided by IMU and velocity provided by optical flow are fused to perform position estimation. Specially, the coordinate system of the first marker in the field is defined as the new world coordinates. The position obtained before the first marker appears needs to be transformed to the new coordinate system. It has been hypothesized that markers have been fixed on the flat ground, so the pitch and roll angles of robot in two coordinates are consistent. Finally, the transformation relationship is as follows:

$$P_m^c = R(\theta_R) P_o^c + T \tag{20}$$

$$\theta_R = \theta_m^c(t) - \theta_o^c(t) \tag{21}$$

$$T = -P_o^c(t) \tag{22}$$

$$R(\theta_R) = \begin{bmatrix} \cos(\theta_R) & \sin(\theta_R) & 0 \\ -\sin(\theta_R) & \cos(\theta_R) & 0 \\ 0 & 0 & 1 \end{bmatrix} \tag{23}$$

where P_o^c and P_m^c are camera position in the initial coordinate system and marker coordinate system, respectively. θ_R is the rotation angle in the z-axis between above two coordinate systems. $\theta_o^c(t)$ and $\theta_m^c(t)$ respectively represent the yaw angle of the camera in the initial coordinate system and marker coordinate at time t. $R(\theta_R)$ and T are the rotation and translation matrices between two coordinate systems.

In addition, depth information measured by the pressure sensor are available at the same sampling frequency as the velocity from optical flow. If the ArUco marker appears in the current frame, the position is easily calculated to correct the accumulative error due to the drift.

IV. GAZEBO-BASED SIMULATION

Simulations are conducted using Gazebo 7 in Robot Operation System (ROS) platform to validate the feasibility and

Authorized licensed use limited to: Harbin Engineering Univ Library. Downloaded on December 01,2021 at 02:26:24 UTC from IEEE Xplore. Restrictions apply.

TABLE III
CAMERA INTRINSIC PARAMETERS

Intrinsic parameters			
f_x	f_y	u_0	v_0
725.9896	725.9038	293.6511	235.3535

TABLE IV
CAMERA DISTORTION PARAMETERS

Distortion parameters				
k_1	k_2	k_3	p_1	p_2
-0.1338	-0.0356	0.2674	-0.00037	-0.0089

TABLE V
NOISE VARIANCES OF VIRTUAL SENSORS

Gyroscope noise variance	$\sim N(0, 0.025)$
Pressure sensor noise variance	$\sim N(0, 0.1)$
Camera noise variance	$\sim N(0, 0.02)$

effectiveness of the proposed self-localization system. Robot model and virtual scene are built in Gazebo platform.

A. Gazebo-Based Simulation Platform

Gazebo is one of the most widely used robot simulation platforms. The robot 3D movement simulation facilitates the robot research. In this simulation, the first step is to design the simulation system, including the robot model establishment and the experimental environment arrangement. We import the model built in SOLIDWORKS into Gazebo to keep the same shape, size, and quality with the real robot. The simulated sensors include IMU, pressure sensor and camera, they are driven by plugins in Gazebo. Camera parameters are the same as those obtained by camera calibration. All the parameters in the simulated experiments have been listed in TABLES III and IV. In order to conform to the actual situation, Gaussian white noises are added to the virtual sensors according to the sensors used in the robot. The noise variances are shown in TABLE V.

The experimental scene design is divided into the water environment and the marker layout. At the bottom of the water environment, 20 ArUco markers with different IDs are fixed for the auxiliary localization of the robot. The simulation environment is shown in Fig.10. Then the next step is to link the localization algorithm on ROS platform with the Gazebo simulation system, as shown in Fig.11. with messages read by the virtual sensors, the robot position is calculated by the state estimation module online, and is fed back to decision center. Using the current position and the predefine trajectory, decision center calculates the control signals using PID algorithm and send control signal to the motors and water-jet thrusters. Since the simulation system and the localization system are completely independent, the format of data transferred between them is the same as the robot prototype, Therefore, all modules in the localization system can be directly applied to the robot prototype.

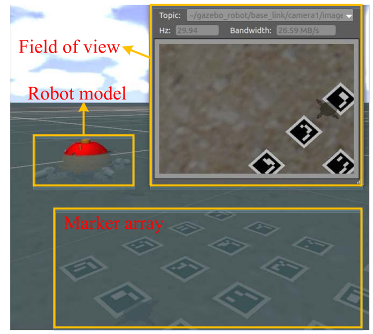

Fig. 10. Simulation environment in Gazebo.

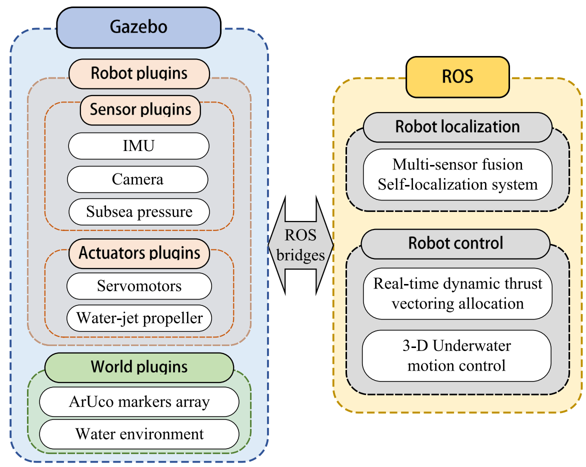

Fig. 11. Structure of simulation platform.

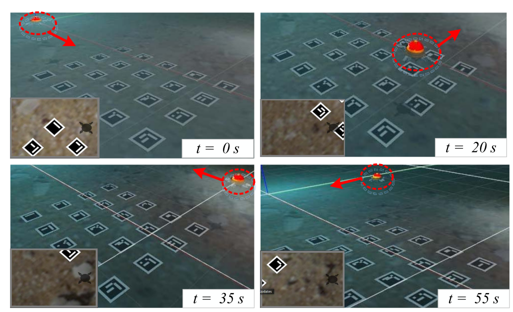

Fig. 12. Motion process and image captured by down-looking camera.

B. Simulation in Gazebo

The robot started from the coordinate origin in the virtual environment, and tracked a counterclockwise rectangle path. While the robot moves along the given path, the down-looking camera detects and recognizes ArUco markers in real time, as shown in Fig. 12. Due to the higher accuracy of markers-based localization, once one marker is recognized, current position is immediately corrected.

Simulated experiments are conducted using two localization methods. In the first method, only IMU and Optical Flow (IOF) are exploited to calculate the robot position.

Authorized licensed use limited to: Harbin Engineering Univ Library. Downloaded on December 01,2021 at 02:26:24 UTC from IEEE Xplore. Restrictions apply.

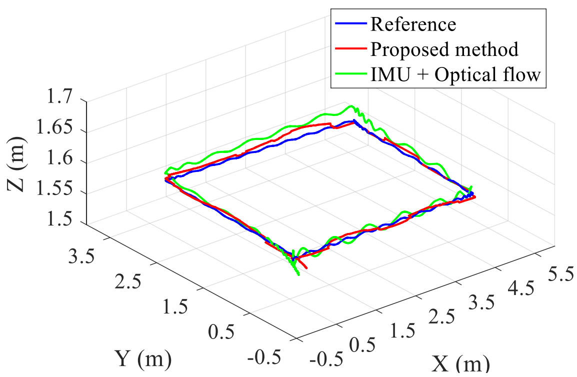

Fig. 13. 3-D estimated trajectory of robot in simulation.

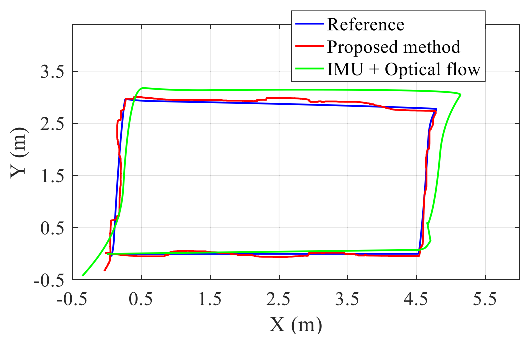

Fig. 14. Estimated trajectory in *X-Y* plane.

The second method is the proposed method which utilizes the ArUco markers to assist localization. 3-D estimated robot trajectory robot in simulation is shown in Fig. 13. The blue, red and green curve indicate the reference, the proposed method and IOF, respectively. Robot trajectories of the two localization methods are generally in the same plane, and the markers-assisted localization method is closer to the preset robot trajectory (blue curve in Fig. 13). Moreover, the localization results with two methods and comparison analysis in 2-D plane are illustrated in Fig. 14 and Fig. 15, respectively. Although the trajectory of IOF method is very smooth and the localization result is close to the reference in a short time, the trajectory deviated from the reference as robot moves. It confirms that the IOF suffer from a drift problem. On the contrary, the marker-aided method can well compensate the drift caused by IOF. As mentioned above, marker information has the highest trust level in our algorithm because it is more reliable than inaccurate optical flow and IMU. Sometimes the output trajectory of the marker-aided method is not very smooth. The reason is that the robot cannot see markers all the time. When there is no valid markers in the view of the robot or recognition failure, IOF will be used to positioning and the estimated localization will gradually diverge from real value due to the drift until the robot catches sight of a marker. At that moment, the position is corrected to an accurate value. This explains why the red curve is not smooth. In the whole trajectory, results of the proposed method at each moment are very close to the preset trajectory, as shown in Fig. 14. According to the analysis of experimental data, IOF

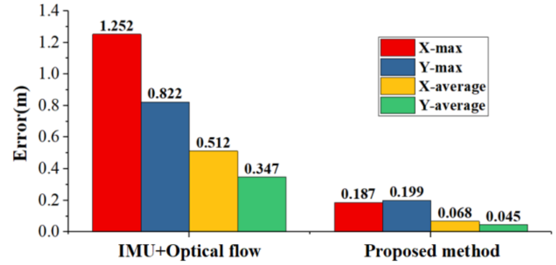

Fig. 15. Maximum and average errors of two methods in simulations.

Fig. 16. (a) Experimental setup and (b) the pre-obtained markers array.

localization results are not very accuracy, and the maximum errors in X and Y are 0.418m and 0.391m over a 15m long trajectory. This is caused by the drift of low cost IMU and optical flow-based velocity estimation. As shown in Fig. 15, the average error of proposed method remains below 10cm and the maximum error is not greater than 20cm, which proves that the proposed method reached the requirement.

Consequently, the proposed method has better performance than the IOF in the average sense. And simulation experiments have demonstrated the availability and accuracy of proposed localization algorithm for the miniature underwater robots with low computational performance and low-cost sensors.

V. Experiments and Analysis

Although simulation results verified the feasibility of the proposed algorithm, a set of experiments employing a miniature robot is conducted to further prove the practicability of the self-localization algorithm. This robot has a good movement performance [33], [34] against water turbulent.

A. Experimental Setup

As this method is designed for the nuclear reactor pool, the turbulent can be ignored. Therefore, experiments were conducted in an indoor swimming pool, with dimensions 3m $\times$ 2m $\times$ 1m as shown in Fig. 16 (a). The bottom of pool was covered with 20 ArUco markers for acquiring precise position information. In the real environment, the light and visibility of water environment will greatly affect the accuracy of marker identification. Thus, in order to detect markers as many as possible, the distribution of markers is relatively dense. And the array and geometry relationship are predefined. The distribution map of markers with different IDs is shown in Fig. 16 (b). A down-looking camera with 640 $\times$ 480 pixels and 30 frames per second (fps) is suspended below the robot, and it is exploited to identify the markers and capture the

Authorized licensed use limited to: Harbin Engineering Univ Library. Downloaded on December 01,2021 at 02:26:24 UTC from IEEE Xplore. Restrictions apply.

TABLE VI
MAIN COMPONENTS OF THE ROBOT

	Item	Features
Sensors	Camera	USB RGB 640 × 480 30 fps
	IMU	Micro Strain 3DM-GX5-45 20Hz
	Pressure sensor	MS5803-14BA 20Hz
Processors	Main Processor	NVIDIA Jetson TK1
	Micro controller	STM32 ARM 32-bit Cotex-M3
Environment	Lab pool with ArUco markers	20 markers with dimensions 16 cm × 16 cm

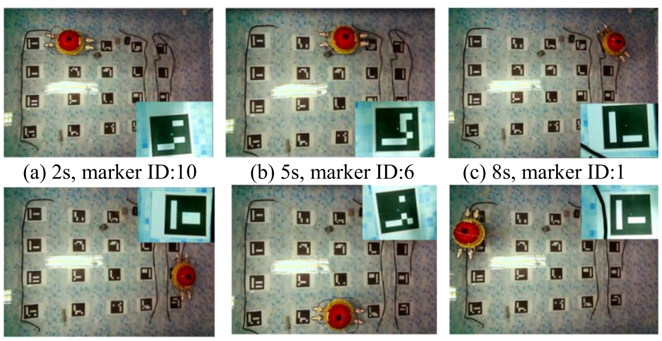

(a) 2s, marker ID:10 (b) 5s, marker ID:6 (c) 8s, marker ID:1
(d) 13s, marker ID:20 (e) 20s, marker ID:8 (f) 28s, marker ID:4

Fig. 17. Snapshots of localization experiment.

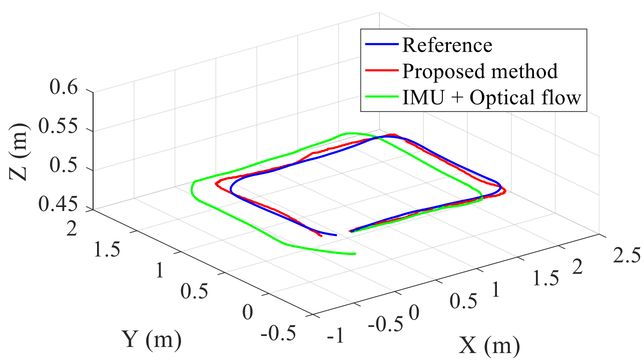

Fig. 18. 3-D estimated trajectory of robot in experiments.

optical flow. A low-cost IMU is fixed in the sealed housing for measuring the yaw, pitch and roll angle of the ego robot. Pressure sensors are used to obtain depth information. Besides, in order to evaluate the robot position calculated by the self-localization method, the global position is estimated using a vision-based localization method with a global camera above the swimming pool. The main hardware and software of localization experiments are summarized in TABLE VI.

B. Localization Performance Analysis and Comparison

This section reports a performance analysis as well as a comparison between the proposed multi-sensor fusion-based algorithm and traditional INS method. In this experiment, a rectangle trajectory is predefined. As shown in Fig.17, the markers were recognized in turn while the robot tracked the trajectory. The 3-D localization results are shown in Fig. 18.

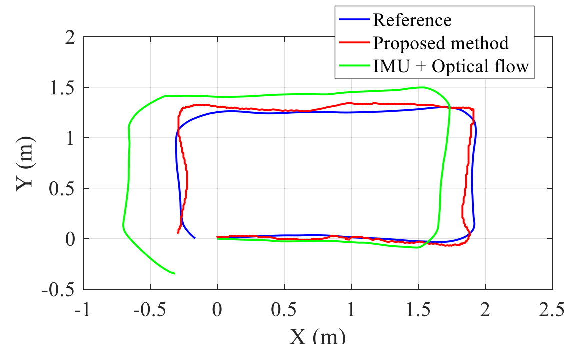

Fig. 19. Estimated trajectory in X-Y plane.

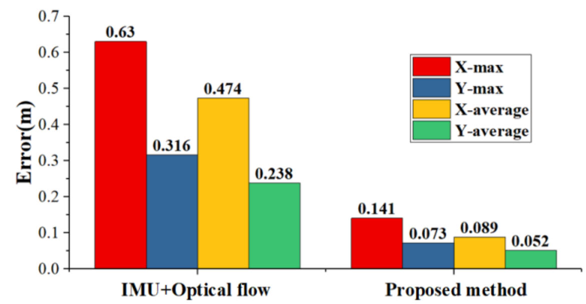

Fig. 20. Maximum and average errors of localization results.

As shown in Fig. 19, the 3-D results are projected to O-XY plane. The red curve indicates the positioning results using the proposed localization method, and the blue curve is the reference calculated by the vision-based localization with a global camera. Compared with the IOF localization results (green curve in Fig. 18), the proposed localization results is closer to the reference, which proves that the proposed marker-aided multi-sensor fusion-based localization method has higher accuracy. Unlike the smooth green curve, the red curve exists fluctuations, which caused by the marker-based position correction. With the marker-based position correction, the deviated robot trajectory is corrected back to the reference. In the z-axis, the two methods have small fluctuations, which conforms to the fact that the robot moves in a defined depth.

To further evaluate the proposed localization results, the maximum error and average error of two methods are compared in Fig. 20. In the 6.5m rectangle trajectory, the maximum errors of IOF in X and Y are 0.613 m and 0.482m, and the maximum errors of the proposed localization method in X and Y are only 0.14m and 0.07m. The errors of IOF came from the error accumulation caused by the drift of IMU and optical flow-based velocity estimation. The errors of the proposed method are mainly caused by the marker identification failure.

In conclusion, as demonstrated by experimental results above, the performance of the marker-assisted multi-sensor fusion-based localization algorithm is significantly better in comparison to the IOF method. Using this proposed method, the miniature robot can position itself online in structured environments. Because of various reasons, marker will not always appear, nor will every marker in the field of view be identified. Nevertheless, information obtained by marker still plays an important role. The estimated position will gradually diverge

Authorized licensed use limited to: Harbin Engineering Univ Library. Downloaded on December 01,2021 at 02:26:24 UTC from IEEE Xplore. Restrictions apply.

until a valid marker is identified. At that moment, the estimated position is enforced to return to an accurate value. Generally, average errors maintain below 10 cm, maximum errors are not greater than 20 cm, which proves that the proposed method reached the requirement.

Compared with simulation results, average errors of the proposed localization method are larger. The reason is that markers identification failure caused by the interference of light in the lab. In contrast, the maximum error in the simulation environment is greater than that in the real environment. The reason for this situation is that the size of the pool limits the moving distance of the robot, and the error accumulation in the localization process is not as obvious as in the simulation. However, the simulation and experimental results have well evaluated and proved the practicability and accuracy of the multi-sensor fusion-based localization method for the miniature underwater robot.

VI. Conclusion

This paper proposed an autonomous underwater self-localization system of a miniature underwater robot using multi-sensor fusion with low computational capacities and low-cost sensors. The proposed multi-sensor fusion method employs Extended Kalman Filter to synthesize the multi-source information from ArUco makers, IMU, pressure sensors and optical flow, which enables the robot obtain a highly precise positioning. This method also can reduce the location drift over time owing to the loss of ArUco markers in pure markers-based localization. Specially, a velocity correction model is built to compensate optical flow-based velocity estimation error using the angles information obtained by IMU. The simulation and experimental results proved that the proposed localization system realized underwater centimeter level positioning, which benefits operation tasks in a structure environment.

Considering the marker recognition failure caused by illumination and occlusion, we will focus on underwater image enhancement to achieve a high recognition rate. Besides, autonomous obstacle avoidance is also to be studied to improve the robot application in the nuclear reactor pool.

References

[1] J. Yan, Z. Xu, X. Luo, C. Chen, and X. Guan, "Feedback-based target localization in underwater sensor networks: A multisensor fusion approach," *IEEE Trans. Signal Inf. Process. Netw.*, vol. 5, no. 1, pp. 168–180, Mar. 2019.

[2] P. S. Rossi, D. Ciuonzo, T. Ekman, and H. Dong, "Energy detection for MIMO decision fusion in underwater sensor networks," *IEEE Sensors J.*, vol. 15, no. 3, pp. 1630–1640, Mar. 2015.

[3] S. Botelho, P. Drews, and G. Leivas, "NLMAP–visual-based self localization and mapping for autonomous underwater vehicles," in *Proc. IEEE Oceans*, Sep. 2008, pp. 1–6, doi: 10.1109/OCEANS.2008.5152106.

[4] Y. Wang, S. Wang, Q. Wei, M. Tan, C. Zhou, and J. Yu, "Development of an underwater manipulator and its free-floating autonomous operation," *IEEE/ASME Trans. Mechatronics*, vol. 21, no. 2, pp. 815–824, Apr. 2016.

[5] Y. Wang, X. Ma, J. Wang, and H. Wang, "Pseudo-3D vision-inertia based underwater self-localization for AUVs," *IEEE Trans. Veh. Technol.*, vol. 69, no. 7, pp. 7895–7907, Jul. 2020.

[6] W. Wang and G. Xie, "Online high-precision probabilistic localization of robotic fish using visual and inertial cues," *IEEE Trans. Ind. Electron.*, vol. 62, no. 2, pp. 1113–1124, Feb. 2015.

[7] L. Shi *et al.*, "An underwater pipeline tracking system for amphibious spherical robots," in *Proc. IEEE Int. Conf. Mechatronics Autom. (ICMA)*, Aug. 2017, pp. 1354–1359.

[8] R. Hartman, W. Hawkinson, and K. Sweeney, "Tactical underwater navigation system (TUNS)," in *Proc. IEEE/ION Position, Location Navigat. Symp.*, May 2008, pp. 898–911.

[9] P. Liu, B. Wang, Z. Deng, and M. Fu, "INS/DVL/PS tightly coupled underwater navigation method with limited DVL measurements," *IEEE Sensors J.*, vol. 18, no. 7, pp. 2994–3002, Apr. 2018.

[10] W. Gao, Y. Liu, B. Xu, and Y. Che, "An improved cooperative localization method for multiple autonomous underwater vehicles based on acoustic round-trip ranging," in *Proc. IEEE/ION Position, Location Navigat. Symp. (PLANS)*, May 2014, pp. 1420–1423.

[11] B. Kuch, G. Buttazzo, E. Azzopardi, M. Sayer, and A. Sieber, "GPS diving computer for underwater tracking and mapping," *Underwater Technol. Int. J. Soc. Underwater*, vol. 30, no. 4, pp. 189–194. 2012.

[12] P. Baccou, B. Jouvencel, V. Creuze, and C. Rabaud, "Cooperative positioning and navigation for multiple AUV operations," in *Proc. MTS/IEEE Oceans Ocean Odyssey Conf.*, Nov. 2001, pp. 1816–1821.

[13] C. Gu, Y. Cong, and G. Sun, "Environment driven underwater camera-IMU calibration for monocular visual-inertial SLAM," in *Proc. Int. Conf. Robot. Autom. (ICRA)*, May 2019, pp. 2405–2411.

[14] A. Kim and R. M. Eustice, "Real-time visual SLAM for autonomous underwater hull inspection using visual saliency," *IEEE Trans. Robot.*, vol. 29, no. 3, pp. 719–733, Jun. 2013.

[15] Z. Yan, P. Gong, W. Zhang, Z. Li, and Y. Teng, "Autonomous underwater vehicle vision guided docking experiments based on L-shaped light array," *IEEE Access*, vol. 7, pp. 72567–72576, 2019.

[16] J. Eisele, Z. Song, K. Nelson, and K. Mohseni, "Visual-inertial guidance with a plenoptic camera for autonomous underwater vehicles," *IEEE Robot. Autom. Lett.*, vol. 4, no. 3, pp. 2777–2784, Jul. 2019.

[17] S. Suresh, E. Westman, and M. Kaess, "Through-water stereo SLAM with refraction correction for AUV localization," *IEEE Robot. Autom. Lett.*, vol. 4, no. 2, pp. 692–699, Apr. 2019.

[18] J. Yu, Z. Wu, X. Yang, Y. Yang, and P. Zhang, "Underwater target tracking control of an untethered robotic fish with a camera stabilizer," *IEEE Trans. Syst., Man, Cybern. Syst.*, vol. 51, no. 10, pp. 6523–6534, Oct. 2021, doi: 10.1109/TSMC.2019.2963246.

[19] R. Wang, S. Wang, Y. Wang, M. Tan, and J. Yu, "A paradigm for path following control of a ribbon-fin propelled biomimetic underwater vehicle," *IEEE Trans. Syst., Man, Cybern. Syst.*, vol. 49, no. 3, pp. 482–493, Mar. 2019.

[20] D. Lee, D. Kim, and H. Myung, "Planar marker-based localization of a robotic fish in a public aquarium," in *Proc. IEEE Int. Conf. Control, Automat. Syst.*, South Korea, Oct. 2011, pp. 448–453, doi: 10.1016/j.proeng.2011.08.408.

[21] M. Carreras, P. Ridao, R. Garcia, and T. Nicosevici, "Vision-based localization of an underwater robot in a structured environment," in *Proc. IEEE Int. Conf. Robot. Autom.*, Sep. 2013, pp. 971–976.

[22] G. C. Karras, P. Marantos, C. P. Bechlioulis, and K. J. Kyriakopoulos, "Unsupervised online system identification for underwater robotic vehicles," *IEEE J. Ocean. Eng.*, vol. 44, no. 3, pp. 642–663, Jul. 2018.

[23] J. Jung, J.-H. Li, H.-T. Choi, and H. Myung, "Localization of AUVs using visual information of underwater structures and artificial landmarks," *Intell. Service Robot.*, vol. 10, no. 1, pp. 67–76, Jan. 2017.

[24] H. Xing *et al.*, "Hybrid locomotion evaluation for a novel amphibious spherical robot," *Appl. Sci.*, vol. 8, no. 2, p. 156, Jan. 2018.

[25] H. Xing *et al.*, "Robust RGB-D camera and IMU fusion-based cooperative and relative close-range localization for multiple turtle-inspired amphibious spherical robots," *J. Bionic Eng.*, vol. 16, no. 3, pp. 442–454, May 2019.

[26] H. Xing *et al.*, "A novel small-scale turtle-inspired amphibious spherical robot," in *Proc. IEEE/RSJ Int. Conf. Intell. Robots Syst. (IROS)*, Nov. 2019, pp. 1702–1707.

[27] X. Hou *et al.*, "Hydrodynamic analysis-based modeling and experimental verification of a new water-jet thruster for an amphibious spherical robot," *Sensors*, vol. 19, no. 2, p. 259, Jan. 2019.

[28] H. Xing, S. Guo, L. Shi, X. Hou, Y. Liu, and H. Liu, "Design, modeling and experimental evaluation of a legged, multi-vectored water-jet composite driving mechanism for an amphibious spherical robot," *Microsyst. Technol.*, vol. 25, no. 8, pp. 1–13, 2019.

[29] S. Garrido-Jurado, R. Muñoz-Salinas, F. J. Madrid-Cuevas, and M. J. Marín-Jiménez, "Automatic generation and detection of highly reliable fiducial markers under occlusion," *Pattern Recognit.*, vol. 47, no. 6, pp. 2280–2292, 2014.

Authorized licensed use limited to: Harbin Engineering Univ Library. Downloaded on December 01,2021 at 02:26:24 UTC from IEEE Xplore. Restrictions apply.

[30] B. Xing, Q. Zhu, F. Pan, and X. Feng, “Marker-based multi-sensor fusion indoor localization system for micro air vehicles,” *Sensors*, vol. 18, no. 6, pp. 1706–1724, 2018.

[31] R. Muñoz-Salinas, M. J. Marín-Jimenez, E. Yeguas-Bolivar, and R. Medina-Carnicer, “Mapping and localization from planar markers,” *Pattern Recognit.*, vol. 73, pp. 158–171, Jan. 2018.

[32] B. D. Lucas and T. Kanade, “An iterative image registration technique with an application to stereo vision,” in *Proc. Int. Joint Conf. Artif. Intell.*, 1981, pp. 674–679.

[33] Y. He, M. Dong, G. Sun, M, Yu, and L. Zhu, “Study on small-scaled amphibious robot with compound driving mechanism and its underwater motion control,” *Chin. J. Sci. Instrum.*, vol. 41, no. 1, pp. 219–226, 2019.

[34] H. Xing *et al.*, “Design, modeling and control of a miniature bio-inspired amphibious spherical robot,” *Mechatronics*, vol. 77, no. 1, pp. 1–16, 2021.

Huiming Xing (Member, IEEE) received the Ph.D. degree in automation from Beijing Institute of Technology, China, in 2020. He is currently a Lecturer with the College of Intelligent Systems Science and Engineering, Harbin Engineering University, China. His current research interests include amphibious bio-inspired robot, underwater spherical robot, soft robotics, vision-based localization, and deep reinforcement learning.

Yu Liu was born in Shanxi, China, in 1997. She received the B.Sc. and M.Sc. degrees in biomedical engineering from the Beijing Institute of Technology, China, in 2017 and 2020, respectively. Her current research interests include indoor localization, multi-sensor information fusion, path planning, and computer vision.

Shuxiang Guo (Fellow, IEEE) received the Ph.D. degree from Nagoya University in 1995. He is currently a Professor in Biomedical Engineering at Beijing Institute of Technology and Kagawa University, Japan. He is also the Leader of the Key Laboratory of Convergence Biomedical Engineering System and Healthcare Technology, Ministry of Industry and Information Technology, China. His research interests include surgical robotics, rehabilitation robotics, endoscopic capsule robotics, and under water robotics. He is the Editor-in-Chief of the *International Journal of Mechatronics and Automation* (IJMA).

Liwei Shi (Member, IEEE) received the Ph.D. degrees in intelligent machine system from Kagawa University, Japan, in 2012, respectively. He was a Postdoctoral Researcher with Kagawa University, Japan. He is currently an Associate Professor with Beijing Institute of Technology, where he researches on underwater micro-robot, such as legged bio-inspired micro-robots, and spherical underwater robots. He has published over 55 refereed journal and conference papers.

Xihuan Hou received the B.S. degree in automation from the North China Institute of Aerospace Engineering, China, in 2014, and the M.S. degree in automation from Harbin Engineering University, China, in 2017. She is currently pursuing the Ph.D. degree in automation with the Beijing Institute of Technology, China. She researches on modeling and control of an amphibious spherical robot, model predictive control, and multi-robot cooperation.

Wenzhi Liu was born in 1968. He has been a Professorate Senior Engineer with the College of Information and Communication Engineering, Harbin Engineering University, since April 2021. His current research interests include underwater robotics and other new unmanned system of oceans.

Yan Zhao (Member, IEEE) received the Ph.D. degree in biomedical engineering from the Beijing Institute of Technology, China, in 2019. He is currently a Lecturer and post-doc in Innovation Team in Key Areas of the Ministry of Science and Technology, School of Mechanical Engineering, Hebei University of Technology. His current research interests include surgical robotics, medical image processing, deep learning, robot learning.

Authorized licensed use limited to: Harbin Engineering Univ Library. Downloaded on December 01,2021 at 02:26:24 UTC from IEEE Xplore. Restrictions apply.